Inorganic Chemistry
Article

Inorg. Chem. **2010**, *49*, 6955–6966 **6955**
DOI: 10.1021/ic1007022

A Surface Effect Allows HNO/NO Discrimination by a Cobalt Porphyrin Bound to Gold

Sebastián A. Suárez,[†] Mariano H. Fonticelli,[‡] Aldo A. Rubert,[‡] Ezequiel de la Llave,[†] Damián Scherlis,[†] Roberto C. Salvarezza,[‡] Marcelo A. Martí,[†,§] and Fabio Doctorovich*[,†]

[†]*Departamento de Química Inorgánica, Analítica y Química Física/INQUIMAE-CONICET, Facultad de Ciencias Exactas y Naturales, Universidad de Buenos Aires, Ciudad Universitaria, Pabellón II, Buenos Aires C1428EHA, Argentina,* [§]*Departamento de Química Biologica, Facultad de Ciencias Exactas y Naturales, Universidad de Buenos Aires, Ciudad Universitaria, Pab. II (1428), Buenos Aires, Argentina, and* [‡]*Instituto de Investigaciones Fisicoquímicas, Teóricas y Aplicadas (INIFTA), Universidad Nacional de La Plata-CONICET, Sucursal 4 Casilla de Correo 16, 1900 La Plata, Argentina*

Received April 12, 2010

Nitroxyl (HNO) is a small short-lived molecule for which it has been suggested that it could be produced, under certain cofactors conditions, by nitric oxide (NO) synthases. Biologically relevant targets of HNO are heme proteins, thiols, molecular oxygen, NO, and HNO itself. Given the overlap of the targets and reactivity between NO and HNO, it is very difficult to discriminate their physiopathological role conclusively, and accurate discrimination between them still remains critical for interpretation of the ongoing research in this field. The high reactivity and stability of cobalt(II) porphyrins toward NO and the easy and efficient way of covalently joining porphyrins to electrodes through S−Au bonds prompted us to test cobalt(II) 5,10,15,20-tetrakis[3-(*p*-acetylthiopropoxy)phenyl]porphyrin [Co(P)], as a possible candidate for the electrochemical discrimination of both species. For this purpose, first, we studied the reaction between NO, NO donors, and commonly used HNO donors, with Co^{II}(P) and Co^{III}(P). Second, we covalently attached Co^{II}(P) to gold electrodes and characterized its redox and structural properties by electrochemical techniques as well as scanning tunneling microscopy, X-ray photoelectron spectroscopy, and solid-state density functional theory calculations. Finally, we studied electrochemically the NO and HNO donor reactions with the electrode-bound Co(P). **Our results show that Co(P) is positioned over the gold surface in a lying-down configuration, and a surface effect is observed that decreases the Co^{III}(P) (but not Co^{III}(P)NO^-) redox potential by 0.4 V.** Using this information and when the potential is fixed to values that oxidize Co^{III}(P)NO^- (0.8 V vs SCE), HNO can be detected by amperometric techniques. Under these conditions, Co(P) is able to discriminate between HNO and NO donors, reacting with the former in a fast, efficient, and selective manner with concomitant formation of the Co^{III}(P)NO^- complex, while it is inert or reacts very slowly with NO donors.

Introduction

Nitroxyl (HNO), the one-electron reduction product of nitric oxide (NO), is a small short-lived molecule that has been intensively investigated in the past decade because of its singular chemical and biological properties.[1−3] More specifically, the reactions of HNO with synthetic metalloporphyrin complexes containing divalent transition metals have been an intense research area in recent years. From the physiological perspective, encouraging studies suggest that HNO can be produced under certain cofactor conditions by NO-producing proteins, the NO synthases.[4−6] Furthermore, several studies have proven distinct pharmacological effects for NO and HNO donors and have shown that the lifetime of HNO in living tissues is probably much longer than previously assumed. This could imply the coexistence of HNO and NO in certain tissues.[7−9] The biologically relevant targets of HNO are mainly heme proteins and thiols.[10,11] HNO is also known

*To whom correspondence should be addressed. E-mail: doctorovich@qi.fcen.uba.ar. Fax: 54-11-4576-3341.

(1) Farmer, P. J.; Sulc, F. *J. Inorg. Biochem.* **2005**, *99*, 166–184.
(2) Miranda, K. M. *Coord. Chem. Rev.* **2005**, *249*, 433–455.
(3) Switzer, C. H.; Flores-Santana, W.; Mancardi, D.; Donzelli, S.; Basudhar, D.; Ridnour, L. A.; Miranda, K. M.; Fukuto, J. M.; Paolocci, N.; Wink, D. A. *Biochim. Biophys. Acta* **2009**, *1787*, 835–840.
(4) Adak, S.; Wang, Q.; Stuehr, D. J. *J. Biol. Chem.* **2000**, *275*, 33554–33561.
(5) Hobbs, A. J.; Fukuto, J. M.; Ignarro, L. J. *Proc. Natl. Acad. Sci.* **1994**, *91*, 10992–10996.
(6) Schmidt, H. H. H. W.; Hofmann, H.; Schindler, U.; Shutenko, Z. S.; Cunningham, D. D.; Feelisch, M. *Proc. Natl. Acad. Sci.* **1996**, *93*, 14492–14497.
(7) Pagliaro, P. *Life Sci.* **2003**, *73*, 2137–2149.
(8) Wink, D. A.; Miranda, K. M.; Katori, T.; Mancardi, D.; Thomas, D. D.; Ridnour, L.; Espey, M. G.; Feelisch, M.; Colton, C. A.; Fukuto, J. M.; Pagliaro, P.; Kass, D. A.; Paolocci, N. *Am. J. Physiol. Heart Circ. Physiol.* **2003**, *285*, 2264–2276.

Published on Web 07/06/2010

to react with molecular oxygen, NO, and HNO itself.[12] These reactions are probably the main sinks of HNO in physiological media.[9] Given the overlap of the molecular targets and reactivity between NO and HNO, it is very difficult to discriminate their physiopathological role conclusively. Cysteine is used in some HNO/NO blocking experiments, but discrimination of both species requires characterization of the final products and cannot be done in situ.[13,14] Clearly, unequivocal discrimination of HNO and NO still remains critical for interpretation of the ongoing research in this field.

As stated above, a number of studies of the HNO reactivity have been performed with metalloporphyrin complexes, generally iron porphyrins, commonly used as heme group models. NO is able to react fast with ferrous and also ferric porphyrins, yielding the corresponding $\{FeNO\}^{6/7}$ complexes according to the Enermark and Feltham notation,[15−17] while HNO reacts with isolated ferric porphyrins and globins to yield $\{FeNO\}^7$ complexes.[18−21] Interestingly, HNO reacts also with ferrous myoglobin and other globins, yielding stable $\{FeHNO\}^8$ complexes.[22,23] The promiscuity of iron porphyrins as well as the reductive nitrosylation reaction that produces $\{FeNO\}^7$ complexes from ferric porphyrins makes them a bad choice for HNO/NO discrimination. However, manganese(III) porphyrins suffer reductive nitrosylation much slower than their iron(III) analogues, allowing one to discriminate HNO from NO in solution.[24] On the basis of this data, Dobmeier et al.[25] designed a Xerogel optical sensor film for quantitative detection of HNO with an estimated dynamic range of 24−290 nM. However, because of the fact that the UV−vis measurements are done in a wavelength range in which all heme proteins strongly absorb, this method cannot be used for most in vitro or in vivo studies. Lippard et al. have developed a fluorescence-based system that uses a copper(II) metallopolymer and is able to discriminate HNO over NO, although it needs a high concentration of HNO donor (ca. 0.3 mM).[26]

Although not studied as much as their iron analogues, cobalt porphyrins also gained prominent attention for the binding and activation of NO. The substitution of iron by cobalt in heme proteins and synthetic porphyrins is an active research field, with synthetic chemistry and biological perspectives. For example, (TPP)Co(NO) (TPP = tetraphenylporphyrin) has been explored as an isoelectronic model for oxygenated protoheme,[27] and the NO adducts of cobalt-substituted myoglobin and hemoglobin have been characterized by electron paramagnetic resonance and UV−vis.[28,29] Several kinetic studies have been done on the NO reaction with cobalt(II) and cobalt(III) porphyrins.[1,30] The specific association rate constants of NO with cobalt(II) porphyrins were estimated to be $k_{on} = 2.0 \times 10^9\ M^{-1}\ s^{-1}$, while the low value of $k_{off} = 1.5 \times 10^{-4}\ M^{-1}\ s^{-1}$ shows the stability of the $Co^{II}NO$ complex, which is actually better represented as a $Co^{III}NO^-$ compound.[30] Interestingly, the association rate of NO with cobalt(III) porphyrins is notably smaller.[30] Last, the redox properties of the NO^- (nitroxyl anion) cobalt porphyrin complexes (TPP)Co(NO) were also studied in organic solvents, such as dichloromethane. Stable complexes of $[(TPP)Co(NO)]^-$ and $[(TPP)Co(NO)]^+$ could be obtained at the electrode surfaces,[31] and redox potentials for Co^{II}-(p-OCH_3)TPP have been reported in several solvents.[32,33]

Metalloporphyrins have also been widely studied for their use in technical applications such as gas sensors[34,35] and catalysts[36−38] when coupled to a surface. Ordered monolayers of porphyrins and metalloporphyrins on inert metal surfaces have been used as convenient model systems for the study of the reactivity and electronic structure of these devices.[39−43] These types of thin-film systems have been used to study direct metalation[39,42,43] and ligand coordination reactions.[41] Interestingly, a recent X-ray photoelectron spectroscopy (XPS) study suggested direct electron transfer from a silver surface to the Co ion from an adsorbed cobalt porphyrin, which could be modulated by coordination of NO to the

(9) Miranda, K. M.; Paolocci, N.; Katori, T.; Thomas, D. D.; Ford, E.; Bartberger, M. D.; Espey, M. G.; Kass, D. A.; Feelisch, M.; Fukuto, J. M.; Wink, D. A. *Proc. Natl. Acad. Sci.* **2003**, *100*, 9196–9201.
(10) Doyle, M.; Mahapatro, S. N.; Broene, R. D.; Guy, J. K. *J. Am. Chem. Soc.* **1988**, *110*, 593–599.
(11) Miranda, K. M.; Nims, R. W.; Thomas, D. D.; Espey, M. G.; Citrin, D.; Bartberger, M. D.; Paolocci, N.; Fukuto, J. M.; Feelisch, M.; Wink, D. A. *J. Inorg. Biochem.* **2003**, *93*, 52–60.
(12) Shafirovich, V.; Lymar, S. V. *Proc. Natl. Acad. Sci.* **2002**, *99*, 7340–7345.
(13) Pino, R. Z.; Feelisch, M. *Biochem. Biophys. Res. Commun.* **1994**, *201*, 54–62.
(14) Shoeman, D. W.; Shirota, F. N.; DeMaster, E. G.; Nagasawa, H. T. *Alcohol* **2000**, *20*, 55–59.
(15) Enemark, J. H.; Feltham, R. D. *J. Am. Chem. Soc.* **1974**, *96*, 5002–5004.
(16) Westcott, B. L.; Enemark, J. H. *Inorganic Electronic Structure and Spectroscopy*; John Wiley & Sons: New York, 1999; Vol. *2*.
(17) Laverman, L. E.; Ford, P. C. *J. Am. Chem. Soc.* **2001**, *123*, 11614–11622.
(18) Bari, S. E.; Marti, M. A.; Amorebieta, V. T.; Estrin, D. A.; Doctorovich, F. *J. Am. Chem. Soc.* **2003**, *125*, 15272–15273.
(19) Suárez, S. A.; Marti, M. A.; De Biase, P. M.; Estrin, D. A.; Bari, S. E.; Doctorovich, F. *Polyhedron* **2007**, *26*, 4673–4679.
(20) Bazylinski, D. A.; Hollocher, T. C. *Inorg. Chem.* **1985**, *24*, 4285–4288.
(21) Bazylinski, D. A.; Hollocher, T. C. *J. Am. Chem. Soc.* **1985**, *107*, 7982–7986.
(22) Kumar, M. R.; Pervitsky, D.; Chen, L.; Poulos, T.; Kundu, S.; Hargrove, M. S.; Rivera, E. J.; Diaz, A.; Colón, J. L.; Farmer, P. J. *Biochemistry* **2009**, *48*, 5018–5025.
(23) Sulc, F.; Immoos, C. E.; Pervitsky, D.; Farmer, P. J. *J. Am. Chem. Soc.* **2004**, *126*, 1096–1101.
(24) Marti, M. A.; Bari, S. E.; Estrin, D. A.; Doctorovich, F. *J. Am. Chem. Soc.* **2005**, *127*, 4680–4684.
(25) Dobmeier, K.; Riccio, D.; Schoenfisch, M. *Anal. Chem.* **2008**, *80*, 1247–1254.
(26) Tennyson, A.; Do, L.; Smith, R.; Lippard, S. J. *Polyhedron* **2007**, *26*, 4625–4630.
(27) Scheidt, W. R.; Hoard, J. L. *J. Am. Chem. Soc.* **1973**, *95*, 8281–8288.
(28) Hori, H.; Ikeda-Saito, M.; Leigh, J. S.; Yonetani, T. *Biochemistry* **1982**, *21*, 1431–1437.
(29) Yu, N.; Thompson, H.; Mizukami, H.; Gersonde, K. *Eur. J. Biochem.* **1986**, *159*, 129–132.
(30) Roncaroli, F.; van Eldik, R. *J. Am. Chem. Soc.* **2006**, *128*, 8042–8053.
(31) Kelly, S.; Lancon, D.; Kadish, K. M. *Inorg. Chem.* **1984**, *23*, 1451–1458.
(32) Walker, F. A. *J. Am. Chem. Soc.* **1970**, *92*, 4235–4244.
(33) Walker, F. A.; Beroiz, D.; Kadish, K. M. *J. Am. Chem. Soc.* **1976**, *98*, 3484–3489.
(34) Guillaud, G.; Simon, J.; Germain, J. P. *Coord. Chem. Rev.* **1998**, *178−180*(2), 1433–1484.
(35) Rakow, N. A.; Suslick, K. S. *Nature* **2000**, *406*, 710–713.
(36) Mochida, I.; Suetsugu, K.; Fujitsu, H.; Takeshita, K. *J. Phys. Chem.* **1983**, *87*, 1524–1529.
(37) Brule, E.; de Miguel, Y. R. *Org. Biomol. Chem.* **2006**, *4*, 599–609.
(38) Zampronio, E.; Gotardo, M.; Assis, M. D.; Oliveira, H. P. *Catal. Lett.* **2005**, *104*, 53–56.
(39) Gottfried, J. M.; Flechtner, K.; Kretschmann, A.; Lukasczyk, T.; Steinruck, H.-P. *J. Am. Chem. Soc.* **2006**, *128*, 5644–5645.
(40) Barlow, D. E.; Scudiero, L.; Hipps, K. W. *Langmuir* **2004**, *20*, 4413–4421.
(41) Williams, F.; Vauhgan, O.; Knox, K. J.; Bampos, N.; Lambert, R. M. *Chem. Commun.* **2004**, 1688.
(42) Kretschmann, A.; Walz, M.; Flechtner, K.; Steinruck, H. P.; Gottfried, J. M. *Chem. Commun.* **2007**, 568.
(43) Auwarter, W.; Weber-Bargioni, A.; Brink, S.; Riemann, A.; Schiffrin, A.; Ruben, M.; Barth, J. V. *ChemPhysChem* **2007**, *8*, 250–254.

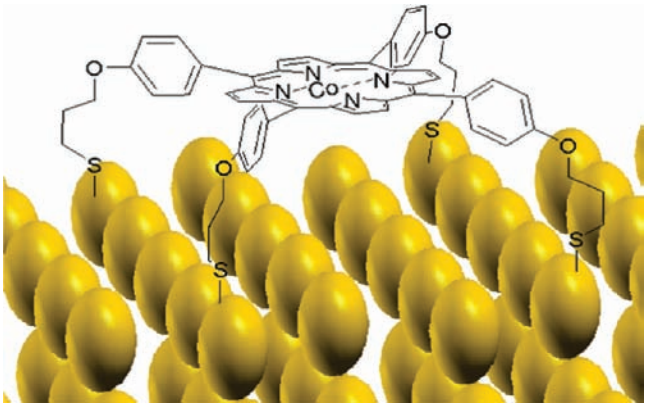

Figure 1. Co(P) adsorbed on a surface.

metal center.[44,45] The most successful methods for surface−molecule linking are based on the establishment of Au−S bonds, and a large number of porphyrin monomers bearing thiols have been prepared and attached to gold electrodes by this method.[46−52] In order to avoid the problems associated with disulfide formation in solution, the thiol is best handled in a protected form (for example, with an *S*-acetyl protecting group),[53,54] that undergoes in situ cleavage on the surface.[48] This technique is easier than evaporation deposition and does not require the use of a quartz microbalance to obtain a single layer.[55]

The high reactivity of cobalt(II) porphyrins toward NO, plus the stability of cobalt(III) porphyrins and the easy and efficient way of covalently joining porphyrins to electrodes, prompted us to test the cobalt(II) 5,10,15,20-tetrakis[3-(*p*-acetylthiopropoxy)phenyl]porphyrin [Co(P)], shown in Figure 1, as a possible candidate for the electrochemical discrimination of both species. For this purpose, first, we studied the reaction between the commonly used HNO donors sodium trioxodinitrate ($Na_2N_2O_3$, Angeli's salt, AS)[56,57] or toluenesulfohydroxamic acid (TSHA), an analogue of Piloty's acid,[58,59] with Co^{II}(P) and Co^{III}(P). We also studied the reaction with NO donors (i.e., NO(g), *N*-nitrosomelatonin).[60,61] Second, we covalently attached Co(P) to gold electrodes and characterized its redox and structural properties by electrochemical techniques as well as scanning tunneling microscopy (STM), XPS, and solid-state density functional theory (DFT) calculations. Finally, we studied electrochemically the NO and HNO donor reactions with the electrode-bound Co(P).

Materials and Methods

Chemicals. Co(P) was purchased from Frontier Scientific and used as received. To study the reaction with HNO, we used AS and TSHA as HNO donors. AS and TSHA were synthesized according to published literature procedures.[62] NO gas was generated by the dropwise addition of a solution containing 280 mg of $NaNO_2$ in 8 mL of degassed water, to a solution of 1.2 g of $FeSO_4 \cdot 7H_2O$ and 0.7 mL of H_2SO_4 in 15 mL of degassed water (see the Supporting Information, reaction scheme SI1). The produced NO was passed through a column of KOH pellets to remove higher nitrogen oxides and through a water scrubbing column prior to use. All these reactions were carried out in an anaerobic atmosphere. *N*-Nitrosomelatonin was prepared as in ref 61. $NaNO_2$ was obtained from Anedra. Ferrocene, $N(Bu)_4PF_6$, and KNO_3 were purchased from Sigma-Aldrich. The remaining chemicals were of analytical grade and were used without further purification. Ethanol, dichloromethane (CH_2Cl_2), and other organic solvents used were spectroscopic grade. The water used was of Milli-Q grade, and nitrogen and argon of high purity were used.

Instruments. Cyclic voltammetry and differential pulse voltammetry (DPV) were carried out with a TEQ 03 potentiostat. For voltammetry in nonaqueous media (CH_2Cl_2), a three-electrode system was used, consisting of two platinum electrodes and a working glassy carbon electrode (GCE), and the supporting electrolyte (SE) was 0.1 M $N(Bu)_4PF_6$. The potential was measured against a ferrocene pseudoreference and converted to standard calomel electrode (SCE) potentials by using $E(\mathrm{SCE}) = E(\mathrm{ferrocene}) + 0.120$ V.

Cyclic voltammetries for the cobalt porphyrin modified electrodes or for the bare gold electrodes used as controls were performed by using the corresponding electrode as the working electrode. In an aqueous solution, a KCl-saturated $Ag^0/AgCl$ electrode was used as the reference electrode and a platinum wire as the counter electrode (SEs were KNO_3 and $KClO_4$, 0.1 M, pH 6). For the corresponding measurements in organic solvent, two platinum electrodes were used. CH_2Cl_2 was distilled from appropriate drying agents (CaH_2) under nitrogen just prior to use. Deaeration of all solutions was accomplished by passing a stream of high-purity argon through the solution for 10 min and maintaining a blanket of inert gas over the solution while making the measurements. The inert gas was saturated with the appropriate solvent before entering the cell to minimize evaporation of the solvent from the cell. Solutions in the cell were changed periodically to avoid contamination from entering the cell via Ag/AgCl because Cl^- anions may interfere.

The midpoint potential ($E_{1/2}$) values were measured as that potential lying midway between the oxidation and reduction peaks for a given couple. Aqueous experiments were carried out at room temperature (~25 °C). CH_2Cl_2 experiments were carried out at room temperature (cathodic waves) and −60 °C (anodic waves). In the last case, an acetone−ethanol slush bath cooled with liquid nitrogen was used to maintain the temperature. In a water solution, the potential was measured against a

(44) Lukasczyk, T.; Flechtner, K.; Merte, L. R.; Jux, N.; Maier, F.; Gottfried, J. M.; Steinruck, H.-P. *J. Phys. Chem. C* **2007**, *111*, 3090–3098.
(45) Flechtner, K.; Kretschmann, A.; Steinruck, H.-P.; Gottfried, J. M. *J. Am. Chem. Soc.* **2007**, *129*, 12110–12111.
(46) Akiyama, T.; Imahori, H.; Sakata, Y. *Chem. Lett.* **1994**, *23*, 1447–1450.
(47) Shimazu, K.; Takechi, M.; Fujii, H.; Suzuki, M.; Saiki, H.; Yoshimura, T.; Uosaki, K. *Thin Solid Films* **1996**, *273*, 250–253.
(48) Gryko, D. T.; Clausen, C.; Lindsey, S. L. *J. Org. Chem.* **1999**, *64*, 8635–8647.
(49) Jagessar, R.; Tour., J. M. *Org. Lett.* **2000**, *2*, 111–113.
(50) Kondo, T.; Ito, T.; Nomura, S.; Uosaki, K. *Thin Solid Films* **1996**, *284−285*, 652–656.
(51) Postlethwaite, T. A.; Hutchison, J. E.; Hathcock, K. W.; Murray, R. W. *Langmuir* **1995**, *11*, 4109–4116.
(52) Simpson, T. R. E.; Revell, D. J.; Cook, M. J.; Russell, D. A. *Langmuir* **1997**, *13*, 460–464.
(53) Lindsey, S. J.; Prathapan, S.; Johnson, E. T.; Wagner, W. R. *Tetrahedron* **1994**, *50*, 8941–8968.
(54) Ravikanth, M.; Strachan, J. P.; Li, F.; Lindsey, J. *Tetrahedron* **1998**, *54*, 7721–7734.
(55) Scudiero, L.; Barlow, D. E.; Mazur, U.; Hipps, K. W. *J. Am. Chem. Soc.* **2001**, *123*, 4073–4080.
(56) Bonner, F. T.; Degani, H.; Akhtar, M. J. *J. Am. Chem. Soc.* **1981**, *103*, 3739–3742.
(57) Gratzel, M. T. S.; Henglein, A. *Ber. Bunsenges. Phys. Chem.* **1970**, *74*, 1003.
(58) Bonner, F. T.; Ko, Y. *Inorg. Chem.* **1992**, *31*, 2514–2519.
(59) Seel, F. C. B. *Z. Anorg. Allg. Chem.* **1972**, *394*, 187–196.
(60) Turjanski, A. G.; Leonik, F.; Estrin, D. A.; Rosenstein, R. E.; Doctorovich, F. *J. Am. Chem. Soc.* **2000**, *122*, 10468–10469.
(61) De Biase, P.; Turjanski, A. G.; Estrin, D. A.; Doctorovich, F. *J. Org. Chem.* **2005**, *70*, 5790–8.
(62) Hughes, M. N.; Cammack, R. *Nitric Oxide, Part C* **1999**, *301*, 279–287.

Ag/AgCl reference and converted to SCE potentials by using $E(\mathrm{SCE}) = E(\mathrm{Ag/AgCl}) + 0.045$ V.

UV−vis spectra were recorded with a HP 8453 spectrometer in a septum-sealed 1-cm-path-length quartz cell.

Electrode Preparation. Before each experiment, the surface of the gold electrode was first polished with alumina powder (diameter, 0.3 and 0.05 μm) and rinsed with pure water. Then this electrode was cleaned in a Piranha solution [2:1 H_2SO_4/H_2O_2 (30% aqueous)] for 5 min. After copious rinsing with Milli-Q water, the gold electrode was electrochemically cleaned by potential cycling in 0.5 M H_2SO_4 in the potential range of 0 and 1.5 V vs Ag^0/AgCl until a typical cyclic voltammogram of clean gold was obtained. After having been rinsed with distilled water, ethanol and dried, the electrode was ready to be modified.

Synthesis of $Co^{III}(P)NO^-$. NO reacts directly with the four-coordinate $Co^{II}(P)$ at room temperature to produce the corresponding five-coordinate $Co^{III}(P)NO^-$ in 75% yield. $Co^{III}(P)NO^-$ was prepared by bubbling NO to 5 mg of $Co^{II}(P)$ dissolved in 3 mL of a degassed 1:1 CH_2Cl_2/MeOH solution. During the course of the addition of NO gas (usually 10−20 min), the color of the reaction mixture changes from purple to red-purple. The reaction was followed by UV−vis spectroscopy until quantitative conversion. The solvent was evaporated and the solid dried in vacuo; the $Co^{III}(P)NO^-$ compound is purple in the solid state. This compound has been characterized by IR (Figure SI1 in the Supporting Information), UV−vis spectroscopy, and microanalysis. Experimental (calcd): C, 62.3% (62.48%); H, 5.0% (4.92%); N, 5.7% (5.69%); S, 10.3% (10.42%). The IR spectrum of the neutral porphyrin shows a strong band at the 1679 cm^{-1} (KBr) region which is assignable to ν_{NO} (Figure SI1 in the Supporting Information). This value is similar to that reported previously for (TPP)Co(NO) (1689 cm^{-1}, KBr)[27] and is close to the range of NO frequencies reported for square-pyramidal N-substituted salicylideaminate complexes of cobalt containing a bent NO ligand (1645−1675 cm^{-1}, Nujol mull).

Reactions of $Co^{III}(P)$ and $Co^{II}(P)$ with HNO and NO Donors. All experiments with $Co^{III}(P)$ were done at 25 °C in a 0.1 M phosphate buffer, containing 10^{-4} M ethylenediaminetetraacetic acid to avoid HNO catalytic decomposition by Cu^{II} and other divalent ions. All experiments with $Co^{II}(P)$ were done at 25 °C in CH_2Cl_2. Porphyrin concentrations were 5×10^{-6} M, unless otherwise noted. All manipulations were performed under an argon atmosphere using septa; solutions were purged for at least 20 min with argon prior to use. All reactions were unaffected by irradiation of the sample with the light source of the spectrometer. AS and TSHA solutions were freshly prepared for each set of measurements and kept on ice, and the concentration was checked before each measurement by UV−vis, following absorbance.[59,63] TSHA was dissolved in 96% ethanol and added to the porphyrin solutions to a final ethanol/water ratio smaller than 1%. NO was produced by using *N*-nitrosomelatonin and a short light flash, as described in previous works from our group.[61] The quantity of NO produced per flash was measured by UV−vis spectroscopy, following *N*-nitrosomelatonin decomposition as previously described.[60] The reaction rates were measured by following the absorbance of the porphyrins at the peak positions of the Soret and/or Q bands. All reactions were pursued until no more spectroscopic changes were observed, unless otherwise stated. The reaction times ranged from 60 s to 2 h.

Immobilization of Co(P) and $Co^{III}(P)NO^-$ on a Gold Surface. For porphyrin adsorption, a solution of 0.5 mg of Co(P) or $Co^{III}(P)NO^-$ in 4 mL CH_2Cl_2 was prepared (0.1 mM). Removal of the *S*-acetyl groups was performed by adding drops of concentrated HCl. The gold surface was immersed in the resulting solution overnight. Finally, the sample was rinsed with CH_2Cl_2, followed by washing with Milli-Q water, and finally dried with an argon stream.

Multilayers of the protected thiol-functionalized Co(P) on Au(111) were prepared by placing a droplet of the 0.1 mM solution of porphyrin in CH_2Cl_2 onto a freshly cleaned gold surface. After all the solvent had evaporated, the sample was measured by XPS without any rinsing procedure at all.

Cystamine Adsorption on a Co(P)-Modified Surface. After porphyrin adsorption, some samples were modified with cystamine. This was carried out by immersing the Co(P)-modified electrodes in a 0.1 M cystamine aqueous solution for 24 h. Finally, the electrodes were rinsed with water, followed by washing with Milli-Q water, and finally dried with an argon stream.

Electrochemical Measurements. The voltammograms of Co(P) were performed before and after the addition of HNO (or NO) donors. The donor solutions were prepared as described above (see section Reactions of $Co^{III}(P)$ and $Co^{II}(P)$ with HNO and NO Donors). When Co(P) is electrochemically driven to the Co^{III} state, the Co^{III}/Co^{II} couple is clearly observed before the addition of an HNO donor. In order to detect the HNO reaction with Co(P), the current was recorded as a function of time (direct-current amperometry), at a fixed potential of 0.8 V, which sets Co(P) in the Co^{III} state, as described in the results.

XPS. Co(P)- and "Co(P) + cystamine"-modified Au(111) samples were analyzed by XPS using a Mg Kα radiation source (XR50, Specs GmbH) and an hemispherical energy analyzer (PHOIBOS 100, Specs GmbH). Previously, two-point calibration of the energy scale was performed using sputter-cleaned gold [Au $4f_{7/2}$; binding energy (BE) = 84.00 eV] and clean copper (Cu $2p_{3/2}$; BE = 933.67 eV) samples. The element ratios were calculated by measurement of the areas corrected by its relative sensibility factors. The reported spectral data were collected with the best possible relation between resolution and sample damage. For the S 2p region spectral deconvolution, a Shirley-type background, and a combination of Lorentzian and Gaussian functions were used. The full width at half-maximum (fwhm) was fixed at 1.1 eV, and the spin−orbit doublet separation of the S 2p signal was set to 1.2 eV. The BEs and peak areas were optimized to achieve the best adjustment.

STM Characterization. For STM imaging, cobalt porphyrins were adsorbed onto preferred oriented Au(111) substrates (from Arrandee's). After annealing for 10 min with a hydrogen flame, these gold substrates exhibit atomically smooth (111) terraces separated by steps, mono- and diatomic in height, as observed by STM. STM imaging was made in air in the constant current mode with a Nanoscope IIE microscope from Digital Instruments (Santa Barbara, CA) and using commercial Pt−Ir tips. Typical tunneling currents, bias voltages, and scan rates were 0.5 nA, 600 mV, and 10−15 Hz, respectively. Calibrations of the piezoscanner for the $x-y$ plane were carried out by imaging highly oriented pyrolytic graphite.[64] Steps present in the Au(111) surface of 0.24 nm height[65,66] were used to calibrate the piezotube in the z direction. Image analysis was carried out using the microscope software, version 5.30r3.sr3 from Digital Instruments. For size distribution analysis, the two-dimensional isotropic power spectral density (PSD) after image high-pass filtering was used.

DFT calculations in periodic boundary conditions were performed using the Quantum Espresso code,[67] which is based on the pseudopotential approximation to represent the ion-electron

(63) Hughes, M. N.; Wimbledon, P. E. *J. Chem. Soc., Dalton Trans.* **1976**, 703–707.

(64) Pong, W.-T.; Bendall, J.; Durkan, C. *Surf. Sci.* **2007**, *601*, 498–509.

(65) Martin, H.; Vericat, C.; Andreasen, G.; Hernandez Creus, A.; Vela, M. E.; Salvarezza, R. C. *Langmuir* **2001**, *17*, 2334–2339.

(66) Bunge, E.; Nichols, R. J.; Roelfs, B.; Meyer, H.; Baumgartel, H. *Langmuir* **1996**, *12*, 3060–3066.

(67) http://www.quantum-espresso.org/.

interactions and plane-wave basis sets to expand the Kohn−Sham orbitals. Ultrasoft-type pseudopotentials[68] were adopted, together with the PBE formalism, to compute the exchange-correlation term.[69] An energy cutoff of 25 and 200 Ry was used to expand the electronic wave functions and the charge density, respectively. The Au(111) surface was modeled as an infinite slab of Au atoms truncated at the (111) geometry, in supercells of dimensions $15.04 \times 11.57 \times 15.04$ Å^3 (Figure SI2 in the Supporting Information). Given the large size of the supercell, required to accommodate the porphyrin molecule, the representation of the surface was limited to two layers of Au atoms, and the sampling of the Brillouin zone was done with a $2 \times 2 \times 1$ Monkhorst−Pack grid.[70] All atomic coordinates were fully relaxed, with the exception of those belonging to the second gold layer, which was frozen on its bulk structure.

Results and Discussion

The results are organized as follows: First, the reactions of Co(P) with HNO and NO are characterized in solution, and electrochemical measurements of Co(P) and $Co^{III}(P)NO^-$ are performed in organic media. Second, Co(P) and Co^{III}-$(P)NO^-$ are covalently bound to gold electrodes, and electrochemical measurements of the modified electrodes are performed. Third, the modified Co(P)-bound electrodes [on Au(111) substrates] are characterized by STM, XPS, and DFT calculations. Finally, the Co(P)-modified gold electrode reactions are studied with NO and HNO to analyze the possibility for the detection and discrimination of both species.

HNO and NO Reactions with Co(P). The initial characterization of the NO and HNO reactions with Co(P) was performed in a CH_2Cl_2 solution using UV−vis spectroscopy. The first reaction was performed by adding NO gas to a $Co^{II}(P)$ solution. The spectral changes observed in CH_2Cl_2 in the Soret and Q bands are shown in Figure 2A, which are in agreement with those reported for other cobalt porphyrins.[30] The conversion of $Co^{II}(P)$ to Co^{III}-$(P)NO^-$ is evidenced after 5 min in the spectrum by a 20 nm shift in the Soret band to higher wavelengths (Figure 2A) and is in agreement with previous data for cobalt porphyrins.[71] In a similar time scale, no spectral changes were observed for $Co^{II}(P)$ in the presence of the HNO donor TSHA.

To study the reaction with $Co^{III}(P)$, we first oxidized $Co^{II}(P)$ using the one-electron oxidant ferrocinium in ethanol as the solvent [$Co^{III}(P)$ is barely soluble in CH_2Cl_2]. After oxidation, excess TSHA was added to $Co^{III}(P)$ in an organic solution under an inert atmosphere, spectral changes corresponding to the conversion of $Co^{III}(P)$ to $Co^{III}(P)NO^-$ were slowly observed (Figure 2B). The half life ($t_{1/2}$) of the reaction under our experimental conditions is 12 min and can be accelerated to less than 1 min by the addition of an organic base (DBU = 1,8-diazabicyclo-[5.4.0]undec-7-ene, 5 μL), which accelerates TSHA decomposition in an organic solvent by deprotonation, as shown previously.[24] In a similar time scale, no spectral changes were observed for $Co^{III}(P)$ in the presence of NO gas or NO donor.

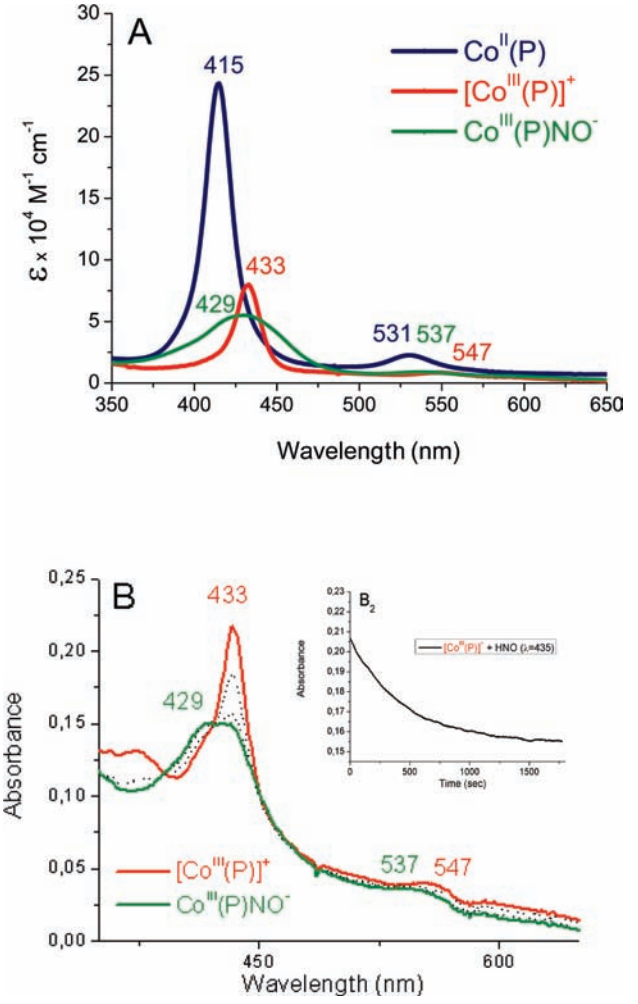

Figure 2. (A) UV−vis spectra of the $Co^{II}(P)$ blue line ($\varepsilon = 2.4 \times 10^5$ M^{-1} cm^{-1}; $\lambda_{max} = 415$ nm), the $[Co^{III}(P)]^+$ red line ($\varepsilon = 8.0 \times 10^4$ M^{-1} cm^{-1}; $\lambda_{max} = 433$ nm), and the $Co^{III}(P)NO^-$ green line ($\varepsilon = 4.9 \times 10^4$ M^{-1} cm^{-1}; $\lambda_{max} = 429$ nm) in CH_2Cl_2. (B) Spectral changes observed for the reaction of $Co^{III}(P)$ with TSHA to yield $Co^{III}(P)NO^-$. Inset: 433 nm peak absorbance vs time plot for the reaction, measured at room temperature in ethanol.

Further confirmation of the $Co^{III}(P)NO^-$ species obtained by the reaction of $Co^{III}(P)$ with TSHA was obtained by isolation and IR measurement of the reaction product, which shows a new narrow band at 1679 cm^{-1} assigned to NO stretching (Figure SI1 in the Supporting Information). Previous results reported by Roncaroli and van Eldik,[30] plus the observed NO stretching band located in a region consistent with NO^-, allow us to unequivocally assign this compound as $Co^{III}(P)NO^-$ instead of Co^{II}-$(P)NO^{\bullet}$, which would be the expected assignment by analogy to FeNO porphyrins. The results clearly show that in solution $Co^{II}(P)$ reacts with NO, and not with HNO, while $Co^{III}(P)$ reacts with HNO and not with NO, as expected.

Cyclic Voltammetry Studies in a CH_2Cl_2 Solution. Prior to the electrochemical measurements of the covalent bound Co(P) to gold electrodes, we characterized the redox properties of Co(P) and $Co^{III}(P)NO^-$ in solution and compared the results with previous data reported for other cobalt porphyrins. Figure 3 shows cyclic voltammograms of both Co(P) and $Co^{III}(P)NO^-$ in CH_2Cl_2/0.1 M

(68) Vanderbilt, D. *Phys. Rev. B* **1990**, *41*, 7892.
(69) Perdew, J. P.; Burke, K.; Ernzerhof, M. *Phys. Rev. Lett.* **1996**, *77*, 3865–3868.
(70) Monkhorst, H.; Pack, J. *Phys. Rev. B* **1976**, *13*, 5188.
(71) Whitten, D. G.; Baker, E. W.; Corwin, A. H. *J. Org. Chem.* **2002**, *28*, 2363–2368.

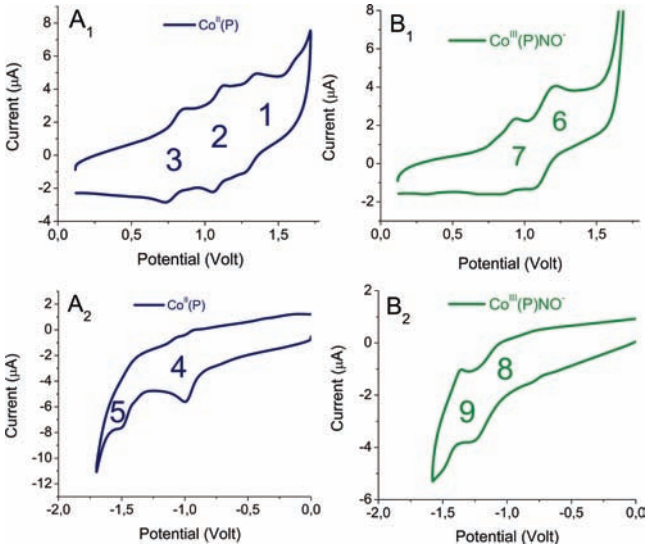

Figure 3. Cyclic voltammograms of Co(P) (left panels A_1 and A_2) and $Co^{III}(P)NO^-$ (right panels B_1 and B_2) in a CH_2C1_2/0.1 M $N(Bu)_4PF_6$ solution (scan rate = 0.1 V s^{-1}). The potential (V) is reported against SCE. In A_1 and B_1, the scan is performed toward positive potentials (measured at room temperature), while in A_2 and B_2, the scan is performed toward negative potentials (measured at −60 °C).

$N(Bu)_4PF_6$. Measurements were performed at both room (20 °C) and low temperature (−60 °C).[72]

As shown in the left panel of Figure 3, five redox couples are found for Co(P), starting from the $Co^{II}(P)$ redox state, corresponding to the following reactions:

$$[Co^{III}(P)]^{3+} + e^- \longleftrightarrow [Co^{III}(P)]^{2+} \quad (1)$$

$$[Co^{III}(P)]^{2+} + e^- \longleftrightarrow [Co^{III}(P)]^{+} \quad (2)$$

$$[Co^{III}(P)]^{+} + e^- \longleftrightarrow Co^{II}(P) \quad (3)$$

$$Co^{II}(P) + e^- \longleftrightarrow [Co^{I}(P)]^- \quad (4)$$

$$[Co^{I}(P)]^- + e^- \longleftrightarrow [Co^{I}(P)]^{2-} \quad (5)$$

The first three reactions (panel A_1) correspond to one-electron oxidations, while the waves shown in A_2 correspond to two one-electron reductions. For $Co^{III}(P)NO^-$, four waves are observed in the right panels of Figure 3 (B_1 and B_2), corresponding to the following reactions:

$$[Co(P)NO]^{2+} + e^- \longleftrightarrow [Co(P)NO]^{+} \quad (6)$$

$$[Co^{III}(P)NO]^{+} + e^- \longleftrightarrow Co^{III}(P)NO^- \quad (7)$$

$$Co(P)NO + e^- \longleftrightarrow [Co(P)NO]^- \quad (8)$$

$$[Co(P)NO]^- + e^- \longleftrightarrow [Co(P)NO]^{2-} \quad (9)$$

The results are consistent with previous measurements of other cobalt porphyrins.[31] As described by Richter-Addo et al.,[72] the nitroxyl porphyrin undergoes two oxidations and two reductions. The $E_{1/2}$ separation for the first oxidation processes for $Co^{II}(P)$ ["Co(P)"] and $Co^{III}(P)NO^-$ ["Co(P)NO", zero global charge] in solution are only 100 mV apart (3,7), and even less for the second. The reduction waves, in solution, are further apart by 340 mV (4,8).

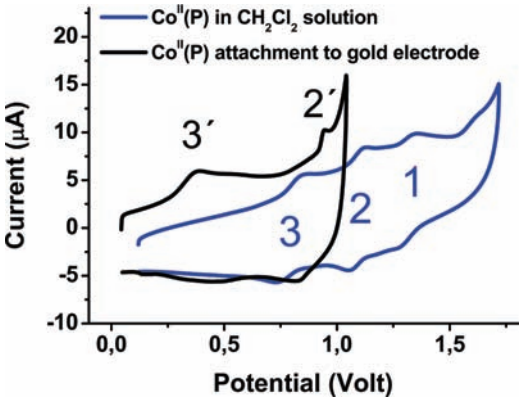

Figure 4. Cyclic voltammograms of Co(P)-modified gold electrodes in a 0.1 M KNO_3/water solution (black line) and Co(P) in a CH_2C1_2/0.1 M $N(Bu)_4PF_6$ solution (blue line). Potential values are referred to SCE (scan rate = 0.1 V s^{-1}).

Porphyrin Attachment and Cyclic Voltammogram Studies of Co(P) Bound to Gold Electrodes. Direct confirmation of Co(P) adsorption was performed by electrochemical measurements of the "Co(P) electrodes" after cleaning of the surfaces with abundant water. XPS data presented in the next section give further insight regarding the presence of Co(P) on gold substrates. Figure 4 shows cyclic voltammograms of the Co(P)-modified gold electrode in a 0.1 M KNO_3 aqueous solution as compared to Co(P) in a CH_2Cl_2 solution [Co(P) is not soluble in water]. Figure 4 shows that a reversible oxidation process is observed within an $E_{1/2}$ value of about 0.4 V. The reaction corresponds to the Co^{III}/Co^{II} couple (reaction 3), and surprisingly the value is shifted ca. 400 mV to lower potentials compared to values in solution. These results show that Co(P) adsorption on the gold electrode facilitates Co^{II} oxidation. The same results were obtained for corresponding electrochemical measurements in a CH_2Cl_2 solution. All resulting computed redox potentials (in solution and adsorbed) are summarized in Table 1.

To confirm that the process corresponds to reduction of the electrode-bound porphyrin, we measured the peak intensities of the process as a function of the scan rate. The resulting plot, shown in Figure SI3 in the Supporting Information, clearly demonstrates that the process corresponds to electrode-bound species.

We then turned to measure HNO-bound Co(P), i.e., $Co^{III}(P)NO^-$. Using the same technique as that for Co(P), $Co^{III}(P)NO^-$ (prepared as described above using NO gas) was covalently attached to gold electrodes and characterized electrochemically. Cyclic voltammograms of "Co^{III}-$(P)NO^-$ electrodes" in a 0.1 M KNO_3 solution show a clear peak corresponding to one-electron oxidation (the inverse of reaction 7) at 0.83 V vs SCE (Figure SI4A in the Supporting Information). In this case, the shift due to the gold surface effect is much smaller than before, only 60 mV. Again, as expected, the intensities show a linear dependence on the scan rate, confirming that the process corresponds to a signal arising from adsorbed species (Figure SI4B in the Supporting Information). Similar results were obtained for the measurements in organic media. All of the resulting $E_{1/2}$ values are summarized in Table 1.

(72) Richter-Addo, G. B.; Hodge, S. J.; Yi, G.-B.; Khan, M. A.; Ma, T.; Van Caemelbecke, E.; Guo, N.; Kadish, K. M. *Inorg. Chem.* **1996**, *35*, 6530–6538.

Table 1. Measured Redox Potentials for Co(P) and $Co^{III}(P)NO^-$

Porphyrin	Solvent – Media / SE	Condition	$E_{1/2}$ (Volt vs. SCE) 1	2, 6	3, 7	4, 8	5, 9[a]
Co(P)	CH_2Cl_2 / $N(Bu)_4PF_6$ 0.1M	Solution[b]	1.29 V	1.09 V	**0.79 V**	-0.80 V	-1.30 V
		Adsorbed[c]	-----	1.10 V	**0.44 V**	- 0.70 V	-----
	Water / KNO_3 0.1 M	Adsorbed[c]	-----	0.90 V	**0.40 V**	-0.79 V	-----
$Co^{III}(P)NO^-$	CH_2Cl_2 / $N(Bu)_4PF_6$ 0.1M	Solution[b]	-----	1.14 V	**0.89 V**	-1.14 V	-1.41 V
		Adsorbed[c]	-----	0.94 V	**0.86 V**	- 1.01 V	------
	Water / KNO_3 0.1 M	Adsorbed[c]	-----	-----	**0.83 V**	- 0.98 V	------

[a] Reaction number. [b] A three-electrode system was used, consisting of two platinum electrodes and a working GCE (scan rate = 0.1 V s^{-1}). Cathodic waves were measured at room temperature and anodic waves at −60 °C. [c] The cobalt porphyrin modified electrodes were used as working electrodes. In aqueous solution, a KCl-saturated Ag^0/AgCl electrode was used as the reference electrode and a platinum wire as the counter electrode. For the corresponding measurements in an organic solvent, two platinum electrodes were used (scan rate = 0.1 V s^{-1}, measured at room temperature).

Table 2. Elemental Ratios for the Co(P) and "Co(P) + Cystamine" Layers on Gold

	N/S	N/Au	N/C	N/O	N/Co
Co(P)	1		0.06	1	4
Co(P) on Au(111)	1.2	0.05	0.04	0.14	5.1
"Co(P) + cystamine" on Au(111)	1.2	0.10	0.05	0.15	7.7

The results from Table 1 show that, due to adsorption of the cobalt porphyrin on the gold surface, a 400 mV decrease in the Co^{III}/Co^{II} couple is observed, and therefore a significant difference in the porphyrin redox potential for the corresponding process is found between the free and NO-bound porphyrins. The resulting first oxidation process occurs at ≈0.4 V for Co^{III}/Co^{II} and at 0.83 V for $Co^{III}(P)NO/Co^{III}(P)NO^-$-modified electrodes in aqueous media. The same results are observed in an organic solvent, showing that this is not a solvent-related but a surface-related effect. Interestingly, the other two redox processes (2 and 4) are not affected by the surface. The origin of the surface effect will be studied further using DFT methods as shown later.

XPS of Co(P) and "Co(P) + Cystamine" Surfaces. In this section, the XPS analysis results of protected Co(P) and "Co(P) + cystamine" on preferred oriented Au(111) substrates are described. The cystamine was used to avoid the reaction as a possible source of a spurious signal in the bare electrode (see below). Table 2 shows the elemental ratios for Au 4f, Co 2p, C 1s, O 1s, and S 2p, in reference to N 1s for the Co(P) (multilayer) and "Co(P) + cystamine" samples. The intensity N/C and N/O ratios exceed the exact molecular stoichiometry. The source of extra oxygen is probably molecular oxygen that can adsorb to the Co center of the molecule.[73,74] Carbon arises not only from the organic molecules but also from contamination during transfer to the UHV chamber. The N/Co ratio, slightly higher than the stoichiometric value for Co(P), indicates some demetalation of loaded porphyrin. For both samples, the N/S ratio is closely above 1, in agreement with the stoichiometric value. These results can be explained assuming that most of the sulfur moieties have been anchored to the gold surface. Therefore, N/S values are greater than 1 because of the signal attenuation of sulfur, which is directly bound to gold and deeper than nitrogen.

Figure 5A shows the presence of N 1s and Co 2p regions for Co(P) on Au(111). A Co $2p_{3/2}$ peak was found at 780.3 eV. The N 1s reveals a main peak (centered at 398.4 eV) and a broad feature at high BE (401.25 eV). Small amounts of metal-free porphyrins could also contribute to this feature, in agreement with some demetalation of Co(P). In addition, contaminants from handling the sample in air might be present.

In the following, the absolute value of the BE of S $2p_{3/2}$ is employed to obtain information about the chemical bonding of the sulfur head to the gold surface. It is worth noting that the S $2p_{3/2}$ core level peak of alkanethiol self-assembled monolayers on gold can be decomposed into three different components: C1 at 161 eV, C2 at 162 eV, and C3 at 163−164 eV.[75] The C1 component is associated with atomically adsorbed sulfur species.[76] Component C2 is related to sulfur chemisorbed on the metal surface through a thiolate bond, while component C3 has been assigned to both unbound thiol and disulfide species.[77−79] The spectral deconvolution of the S 2p region (Figure 5B,

(73) Berner, S.; Lidbaum, H.; Ledung, G.; Åhlund, J.; Nilson, K.; Schiessling, J.; Gelius, U.; Bäckvall, J.-E.; Puglia, C.; Oscarsson, S. *Appl. Surf. Sci.* **2007**, *253*, 7540–7548.
(74) Yoshimoto, S.; Suto, K.; Tada, A.; Kobayashi, N.; Itaya, K. *J. Am. Chem. Soc.* **2004**, *126*, 8020–8027.
(75) Vericat, C.; Vela, M. E.; Benitez, G. A.; Gago, J. A. M.; Torrelles, X.; Salvarezza, R. C. *J. Phys.: Condens. Matter* **2006**, *18*, R867–R900.
(76) Yang, Y. W.; Fan, L. J. *Langmuir* **2002**, *18*, 1157–1164.
(77) Heister, K.; Zharnikov, M.; Grunze, M.; Johansson, L. S.; Ulman, A. *Langmuir* **2000**, *17*, 8–11.
(78) Zhong, C.-J.; Brush, R. C.; Anderegg, J.; Porter, M. D. *Langmuir* **1998**, *15*, 518–525.
(79) Ishida, T.; Choi, N.; Mizutani, W.; Tokumoto, H.; Kojima, I.; Azehara, H.; Hokari, H.; Akiba, U.; Fujihira, M. *Langmuir* **1999**, *15*, 6799–6806.

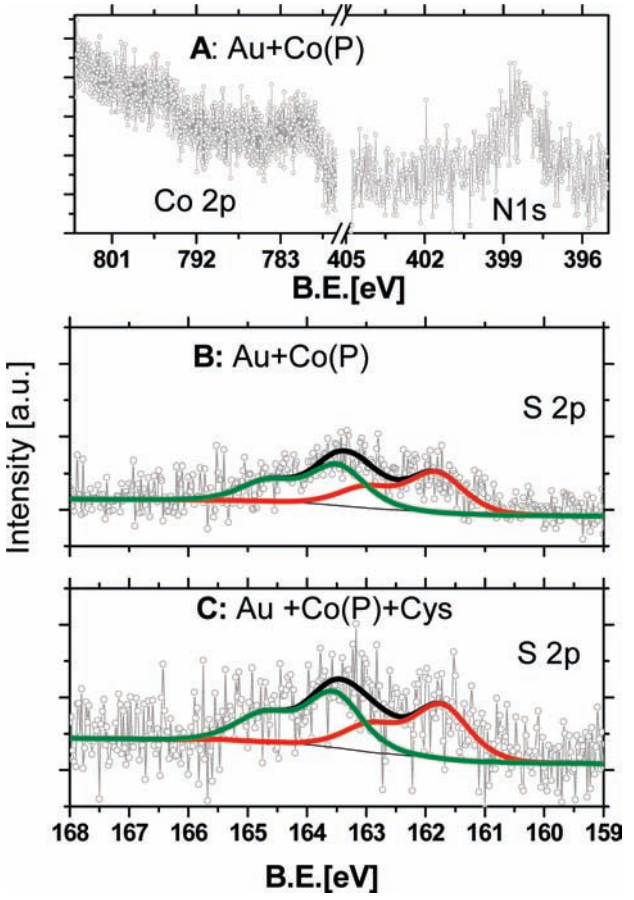

Figure 5. XPS spectra of (A) the Co 2p and N 1s regions, (B) the S 2p region for Co(P) on Au(111), and (C) S 2p regions for "Co(P) + cystamine" on Au(111). The S 2p regions are shown as two peak deconvolutions for both samples.

C) shows two components of BEs at 161.9−162.1 eV (C2) and 163.3−163.4 eV (C3). The C2 component corresponds to a p doublet of thiolates bound to gold, while the C3 contribution is related to free thiol, thioacetyl functions, and disufides. Similar results were obtained for acetyl-protected porphyrin adsorption from solution[73,80] and under ultrahigh-vacuum conditions.[81] It is worth noting that it is not clear which fraction of the C3 component is related to any of the species that contribute to this signal. Whatever was the origin of this component, it is clear that it seems to be about half of the total sulfur amount. Then, it might be claimed that Co(P) could be adsorbed with its porphyrin ring both parallel to the surface or near to its surface normal. In this sense, Berner et al. carried out XPS measurements at different takeoff angles, establishing that the thioacetyl or free thiols are located in the outermost parts of the surface.[73,80] If this is true for the current system, which makes sense, the bound sulfur amount should be estimated considering some attenuation. Then, it is reasonable to suppose that the number of sulfur species attached to the substrate is greater than that corresponding to C3 related species. Under this circumstance, the lying-down configuration

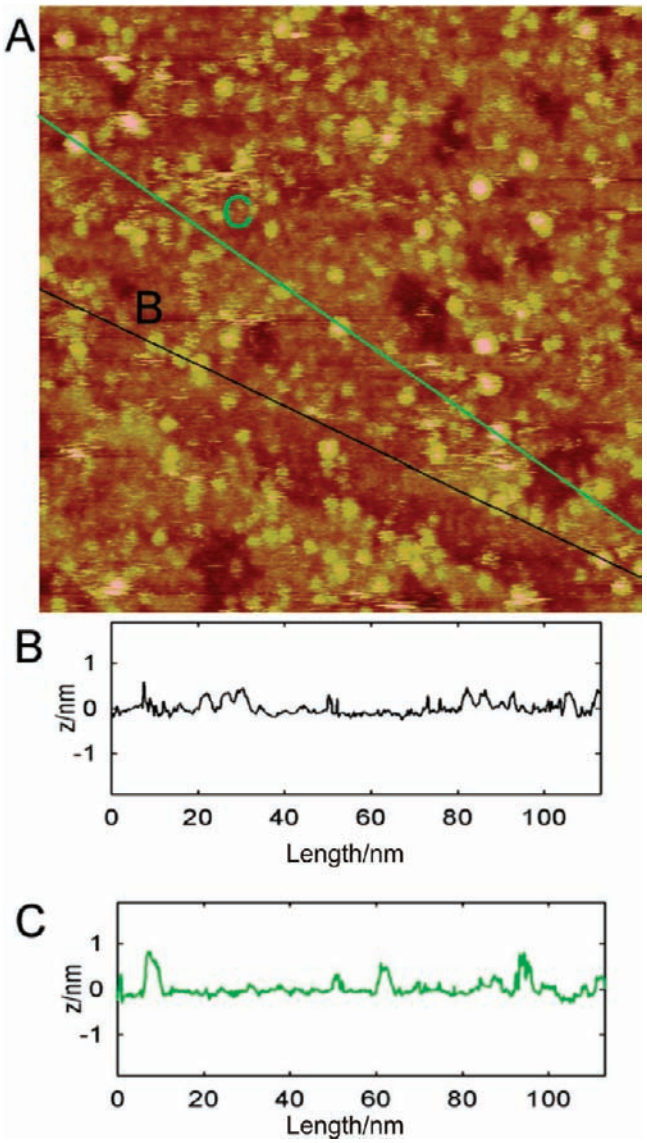

Figure 6. (A) 100 nm × 100 nm STM image of a Co(P)-modified Au(111) substrate. (B) Cross-sectional profile corresponding to the black trace on Figure 6A. (C) Cross-sectional profile corresponding to the green trace on Figure 6A.

would be, on average, favored. We found further support in favor of molecules having their porphyrin ring parallel to the surface by carrying out STM imaging of Co(P)-modified surfaces (see below).

XPS analysis indicates an increase in the S/Au and N/Au intensity ratios after cystamine adsorption. Considering that during cystamine adsorption each molecule gives rise to two thiols after breakage of the S−S[82] bond, this result shows that free gold sites are probably blocked. No oxidized sulfur species (S 2p BE > 166 eV) such as sulfonate were detected by XPS on any of the analyzed samples.

Characterization of a Co(P)-Bound Gold Surface by STM. We also characterized the covalently bound Co(P) at the molecular level by STM imaging. This is a key point regarding the chemical activity of immobilized molecules because it strongly depends on the porphyrin overlayer structure and on the adsorption geometry of individual

(80) Berner, S.; Biela, S.; Ledung, G.; Gogoll, A.; Backvall, J.; Puglia, C.; Oscarsson, S. *J. Catal.* **2006**, *244*, 86–91.
(81) Turner, M.; Vaughan, O. P. H.; Kyriakou, G.; Watson, D. J.; Scherer, L. J.; Davidson, G. J. E.; Sanders, J. K. M.; Lambert, R. M. *J. Am. Chem. Soc.* **2009**, *131*, 1910–1914.
(82) Wirde, M.; Gelius, U.; Nyholm, L. *Langmuir* **1999**, *15*, 6370–6378.

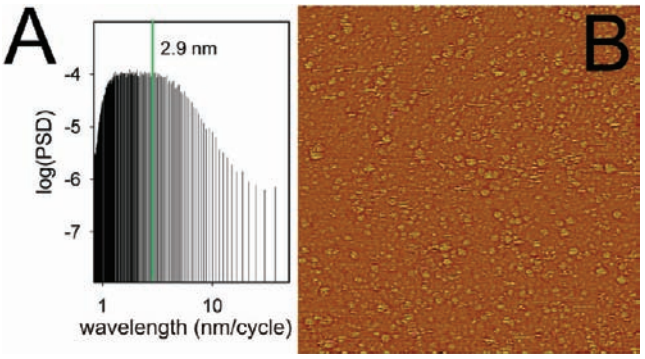

Figure 7. (A) PSD plot obtained by analysis of the image on panel "B". Notice that both the power and wavelength are indicated on logarithmic scales. (B) 150 nm × 150 nm images of Co(P) species adsorbed on a Au(111) terrace, after high-pass filtering.

molecules. Typical STM images of the Co(P)-covered Au(111) surfaces are shown in Figure 6A. A step edge between two Au(111) terraces across the image is visible near the left-down corner (parallel to the black line indicated as "B"). Also, vacancy gold islands, which are frequently observed on thiol-modified surfaces, in the atomically smooth terraces of the Au(111) substrate can be clearly distinguished. The substrate is decorated by a large number of randomly distributed bright spots, which are related to porphyrin adsorption. Figure 6 shows that there are two types of elements, the most frequently observed are 0.42 ± 0.11 nm in height (cross section, Figure 6B), while the larger and brighter ones exhibit 0.87 ± 0.08 nm height (cross section, Figure 6C; see also the height histogram included in Figure SI5 in the Supporting Information). The 0.4 nm heights are in good agreement with previously reported data about molecular contrast in STM images of metal-modified porphyrins[74,83] and phthalocyanines.[84] The brighter spots with heights of about 0.9 nm can be assigned to agglomerates in a second layer. In fact, it has been shown that porphyrins are able to form bilayers.[74,83] If the molecules were oriented with their porphyrin plane near the surface normal, they should show an apparent height of about 3 nm. Furthermore, this supposition is still valid for the brightest spots (associated porphyrin). The possibility of having porphyrin aggregates, in which not all of the mercapto functions are covalently bound to the substrate, is consistent with the XPS results, which show contributions of acetyl-protected thiols, unbound thiols, or disulfides to the sulfur signal. Repetitive scanning with the STM tip did not remove the molecules, indicating that they are strongly bound to the gold surface and also that the second layer is firmly attached to the first one.

Regarding the porphyrin orientation with respect to the surface, the apparent porphyrin size in the $x-y$ plane was analyzed. Two-dimensional PSD analysis of a 150 nm × 150 nm image, after high-pass filtering, shows a broad distribution of spots with average size 2.9 nm (Figure 7A).

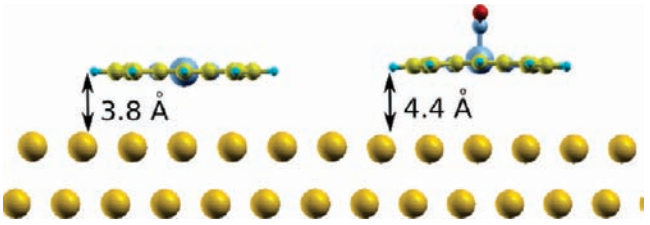

Figure 8. Structures of Co(P) and $Co^{III}(P)NO^-$ on the Au(111) surface optimized by DFT calculations.

These 2.9-nm-sized spots are consistent with similar cobalt porphyrins chemisorbed on gold surfaces.[85] This also suggests that the molecules are in the lying-down configuration.

From XPS and STM analysis of the modified surfaces, it can be inferred that most of the Co(P) molecules are adsorbed in the lying-down configuration by multiple-linker binding to the gold surface, with some molecules in a second layer. The strong adsorbate−surface interaction explains the random distribution of porphyrins through the Au(111) terraces. Consequently, considering that a disordered Co(P) adlayer had been grown, vacant gold sites can be occupied by adsorbates having a smaller lateral size. These findings would also be expected to be valid in the case of porphyrin immobilized on the polycrystalline electrodes used in the electrochemical experiments.

To compute the surface coverage, reductive desorption[86,87] of the thiolated porphyrins was performed in basic media (0.1 M KOH). From the cathodic peak in the voltammogram (Figure SI7 in the Supporting Information), the charge density involved in thiol reduction was measured. The charge density value allows estimation of the number of porphyrin molecules present on the gold surface, assuming one electron per thiolate bond. The resulting calculation yields a surface coverage of 25% (see the Supporting Information for more details on the calculation). This value is similar, within experimental error, to the one obtained using STM. We have also verified from voltammetric runs that there was no significant adlayer degradation after potential excursion to 1.0 V in a 0.1 M KNO_3 aqueous solution.

Electronic Structure Calculations of Co(P) and Co^{III}(P)NO^-. Model structures of the Co(P) and $Co^{III}(P)NO^-$ complexes resting on the Au(111) surface were optimized by using DFT calculations. Geometry relaxations were started from equivalent configurations for both systems, with the porphyrin macrocycles lying about 3.7 Å above the surface. Interestingly, the optimizations led to the final structures depicted in Figure 8: the average lengths from the first gold layer to the plane of the molecule turned out to be 3.79 and 4.43 Å for the free and nitrosylated porphyrins, respectively. The separation obtained for the Co(P) model is in reasonable agreement with the value observed from the STM adsorbates, of 0.42 ± 0.11 nm. The Co atoms sits between two Au atoms on a bridge site.

The atomic charges resulting from a Lowdin population analysis are shown in Table 3. In Co(P), the charge on

(83) Yoshimoto, S.; Suto, K.; Honda, Y.; Itaya, K. *Chem. Phys.* **2005**, *319*, 147–158.
(84) Hipps, K. W.; Lu, X.; Wang, X. D.; Mazur, U. *J. Phys. Chem.* **1996**, *100*, 11207.
(85) Berner, S.; Ledung, G.; Ahlund, J.; Nilson, K.; Schiessling, J.; Gelius, U.; Backvall, J.-E.; Puglia, C.; Oscarsson, S. *Appl. Surf. Sci.* **2007**, *253*, 7540–7548.
(86) Walczak, M. M.; Popenoe, D. D.; Deinhammer, R. S.; Lamp, B. D.; Chung, C.; Porter, M. D. *Langmuir* **1991**, *7*, 2687–2693.
(87) Yang, F.; Wilde, C. P.; Morin, M. *Langmuir* **1996**, *12*, 6570–6577.

the metal becomes less positive upon binding. In contrast, the cobalt charge increases slightly in $Co^{III}(P)NO^-$ when the molecule approaches the gold surface. This behavior is indicative of the different nature of the Co−Au interaction in the presence and in the absence of NO. At the same time, some electron density seems to flow away from the porphyrin N atoms in Co(P), while the atomic populations of the equatorial N atoms are hardly affected when NO is bound. We can conclude that NO coordination separates the porphyrin from the gold surface and diminishes the charge transfer from the surface to the Co center, consistent with what was previously reported by Flechtner et al. for a gold surface.[45]

HNO and NO Detection and Discrimination Using Co(P)-Modified Gold Electrodes. As mentioned in the introduction, the main aim of this study is to develop a device that is able to detect and discriminate HNO from NO, using Co(P). To achieve this goal, the Co(P)-modified electrode must be able to react with HNO but not with NO (or any other similar species) and yield an electrochemical response in the presence of HNO. Alternatively, an NO-selective detector must react with NO but not with HNO. Given the known reactivity in solution, which shows that $Co^{II}(P)$ reacts fast with NO but not with HNO while the opposite is observed for $Co^{III}(P)$, we tested both reactions for the Co(P)-modified gold electrodes. The reactions were monitored electrochemically using the same protocol as that mentioned above. For example, to analyze the $Co^{III}(P)$ reaction with HNO or NO, a voltammogram of Co(P) was performed before and after the addition of an HNO (or NO) donor, as shown in Figure 9A. When Co(P) is electrochemically driven to the Co^{III} state, the Co^{III}/Co^{II} couple is observed before the addition of AS (blue line, 0.4 V). Under the same conditions [oxidized Co(P)], adding AS results in a shift of the voltammogram corresponding to $Co^{III}(P)NO^-$ (green line, 0.83 V). This clearly shows the in situ reaction of $Co^{III}(P)$ with HNO. To verify that the shift is due to a surface effect and that it is not affected by the SE, the same experience was performed but with 0.1 M $KClO_4$ (pH 6). In turn, because the redox event observed was pseudoreversible (green line in Figure 9A), the apparent potentials were measured more carefully by DPV techniques (Figure 9B).

Using similar procedures, the rest of the reactions (listed below) were studied. As expected, the results show that $Co^{III}(P)$ reacts efficiently with HNO, while it does not with NO donors or NO gas. This is evidenced by the lack of electrochemical signals (current intensity) when the porphyrin is maintained in the Co^{III} state, at a potential compatible with the $Co^{III}(P)NO/Co^{III}(P)NO^-$ couple (about 0.8 V), and the current intensity is monitored after the addition of NO donors. On the other hand, NO reacts rapidly with $Co^{II}(P)$-modified electrodes while HNO does not; i.e., the $Co^{III}(P)NO/Co^{III}(P)NO^-$ couple is observed after the addition of an NO donor to a Co(P)-bound electrode maintained in the $Co^{II}(P)$ state, while no change is observed when HNO donors are used. The resulting behavior of the modified electrodes is summarized in Scheme 1.

A very important issue for selective HNO detection in the presence of NO is the fact that NO is able to react with bare gold electrodes at 0.8 V. Therefore, it is necessary to avoid this reaction as a possible source of spurious signals. To study the NO response on the Co(P)-modified electrodes, we measured the current intensities produced by a 3 μM NO solution on (a) bare gold electrodes (green curve on Figure 10), (b) Co(P)-modified electrodes (red

Table 3. Atomic Charges According to a Lowdin Population Analysis, for the Relaxed Structures of Co(P) and $Co^{III}(P)NO^-$ in a Vacuum (isolated) and on the Au(111) Surface (Adsorbed)[a]

		Co	$\sum N_p$	$\sum NO$
Co(P)	isolated	+0.83	-1.00	-
	adsorbed	+0.78	-0.89	-
$Co^{III}(P)NO^-$	isolated	+0.73	-0.89	+0.06
	adsorbed	+0.77	-0.87	+0.12

[a] $\sum N_p$ and $\sum NO$ stand for the charges summed on the porphyrin N atoms and on the HNO atoms, respectively.

Scheme 1

$Co^{II}(P) + NO \longrightarrow Co^{III}(P)NO^-$

$Co^{II}(P) + HNO \longrightarrow$ No reaction

$Co^{III}(P) + HNO \longrightarrow Co^{III}(P)NO^-$

$Co^{III}(P) + NO \longrightarrow$ No reaction

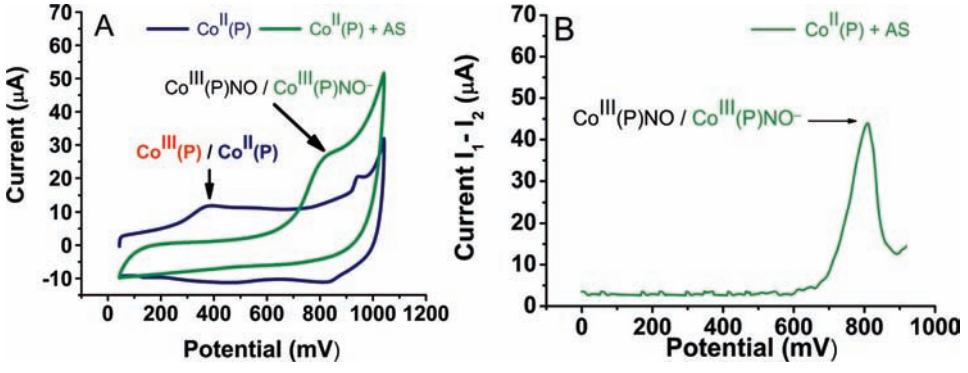

Figure 9. In situ HNO reaction with adsorbed $Co^{III}(P)$. Potential values are referred to SCE (scan rate = 0.1 V s^{-1}). (A) Cyclic voltammograms of $Co^{III}(P)$ before (blue line) and after (green line) the addition of 0.7 mM AS in a 0.1 M KNO_3 aqueous solution. (B) DPV of $Co^{III}(P)$ after the addition of 0.7 mM AS in a 0.1 M $KClO_4$ aqueous solution. Pulse amplitude: 30 mV. Pulse width: 25 ms. Pulse period: 40 ms.

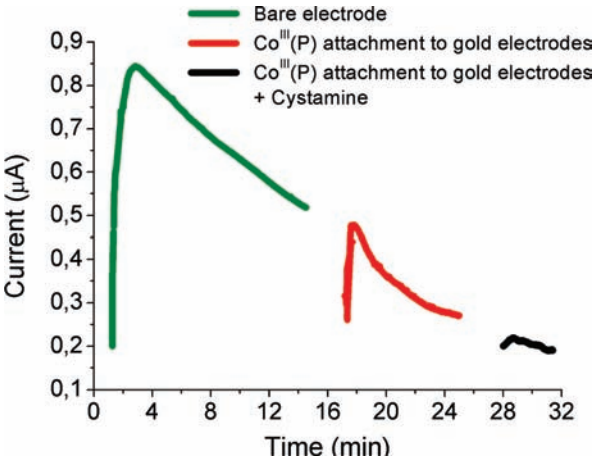

Figure 10. Current intensity for 3 μM NO on bare gold electrodes (green), Co^{III}(P)-modified electrodes (red), and "Co^{III}(P) + cystamine"-modified electrodes (black). The current was detected by fixing the electrode potential at 0.8 V vs SCE.

Scheme 2

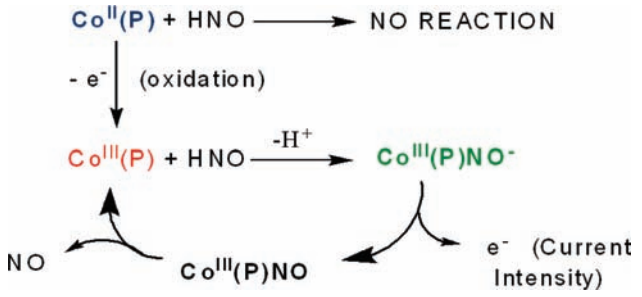

curve on Figure 10), and (c) "Co(P) + cystamine"-modified gold electrodes (black curve on Figure 10). NO was produced by using *N*-nitrosomelatonin and a short light flash.[55] The quantity of NO produced per flash was measured by UV−vis spectroscopy. The signal was recorded by fixing the potential at 0.8 V and measuring the current versus time after NO addition.

As shown in Figure 10, a considerable current intensity is observed because of the presence of 3 μM NO in solution when bare gold electrodes are used as working electrodes. The Co(P) porphyrin partially blocks the signal (the remaining signal is ca. 50% of that for the bare electrode), although because of the 25% coverage of the gold surface by Co(P), the signal is still significant. To completely block the signal coming from the direct interaction of NO with gold sites, the Co(P)-modified electrodes were subsequently modified with cystamine. As expected, for these electrodes, the current intensity dropped to less than 5% of the original one, proving that the reaction of NO with the electrode is almost completely avoided. Finally, we verified that cystamine does not interfere with the Co^{III}(P)NO$^-$ electrochemical signal, as shown in Figure SI8 in the Supporting Information.

HNO Detection. In order to detect HNO, the following reaction scheme was designed (Scheme 2), on the basis of the previous electrochemical data. According to Scheme 2, in order to selectively detect HNO, the resting-state electrode potential is set to 0.8 V. At this value, Co(P) is stable in the Co^{III}(P) state and no current flow is observed. The reaction with HNO yields, according to

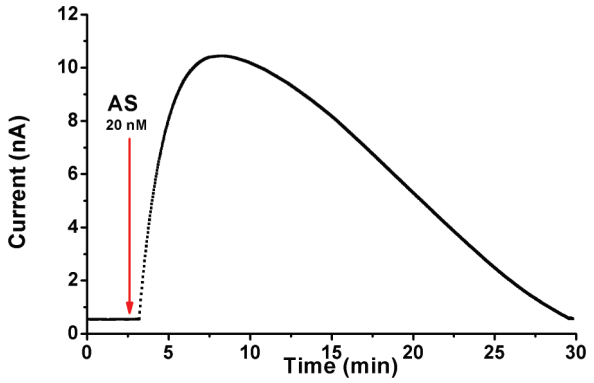

Figure 11. Intensity vs time plot for Co(P)-modified electrodes. The arrow indicates the addition of AS.

previous observations, Co^{III}(P)NO$^-$, which under the described conditions is oxidized to Co^{III}(P)NO. The Co^{III}(P)NO complex releases the NO ligand to yield Co^{III}(P), which allows the catalytic cycle to start again.

The measured current corresponds to oxidation of Co^{III}(P)NO$^-$ at 0.8 V, as is nicely shown in Figure 11, which is detected only a few seconds after AS addition. It should be noted that a fast equilibrium between the continuous HNO production by AS decomposition and HNO dimerization occurs, yielding a steady-state HNO concentration that reacts with Co^{III}(P), as is further explained below.

As can be observed from Figure 11, the obtained current intensity increases after the addition of the HNO donor, in about 2−3 min. After this initial signal increase, the current starts to decay slowly because of the expected AS decomposition,[20] with a half-life in the range of AS to HNO decomposition under these conditions ($t_{1/2}$ = 15 min, at pH 7 and room temperature).[20] The coincidence of the current signal decay times with AS spontaneous decomposition decay to yield HNO strongly suggests that Co(P) is reacting with the released HNO as expected. To analyze the quantitative response of the electrode upon AS addition, we measured the current intensity obtained by the addition of different initial AS concentrations at 0.8 V. The minimum HNO detection limit of the electrode under our experimental conditions is ca. 1 nM, corresponding to a current of 3.65 nA. The concentration of HNO was estimated as described in the Supporting Information.

We also performed the same set of experiments without stirring of the solution, although in this case the HNO reaction with the electrode is limited by diffusion and the intense signal obtained after AS addition falls off rapidly after an initial burst of reaction, possibly because of limited HNO diffusion to the surface. These results are shown in Figure SI9 in the Supporting Information. Finally, to corroborate the selectivity of the method, the current of the same Co(P) electrode (in the same conditions) was measured after the addition of an NO donor. As expected, no increase in the current intensity was observed because of the lack of reaction of Co^{III}(P) with NO, showing the HNO selectivity of the presented method.

Conclusions

Redox Potential Shift for the Co^{III}/Co^{II} Gold-Adsorbed Porphyrin. One of the most interesting points observed in

this work is the 400 mV shift of the redox potential for the Co^{III}/Co^{II} redox couple when comparing the cobalt porphyrin in solution with the adsorbed species, while only a very small shift is observed for the nitrosylated $Co^{III}(P)NO/Co^{III}(P)NO^-$ couple. In an interesting work by Lukasczyk et al., by using XPS, evidence of electron transfer from a silver surface to the Co metal center of an electrostatically adsorbed porphyrin was obtained.[44] They also showed that the above-mentioned Co−Ag interaction is suppressed by axial coordination of NO to the cobalt porphyrin, and the authors suggested that this effect results from competition between the two axial ligands (NO and the silver surface, considered as a "ligand").[45] Electronic coupling between the Co center of a porphyrin and a metal surface has also been observed by using STM.[40,51,52,88] Our electrochemical measurements are in agreement with a surface-to-porphyrin charge donation and the suppression of this effect by NO coordination. In the noncoordinated porphyrin, charge donation from the surface significantly stabilizes the Co^{III} state, lowering the Co^{III}/Co^{II} redox potential compared to the value in solution. The difference of about 0.6 Å in the surface separation obtained by DFT calculations for the free and nitrosylated porphyrins is a direct evidence of the role of NO in the weakening of the Co−Au interaction. In the particular case of $Co^{III}(P)NO^-$, where the ligand pulls the metal out of the plane, the distance between the slab and the Co atom is 4.64 Å, too large to expect any significant coupling between the cobalt and the surface. NO coordination suppresses most of the charge-transfer effect, and therefore no significant change in the redox potential is observed between $Co^{III}(P)NO^-$ in solution and the adsorbed species. The decrease of 0.05 e^- in the calculated atomic charge of the Co metal center upon adsorption of $Co^{II}(P)$ supports the notion of electron transfer from the surface to the metal center. This is accompanied by an increase of the charge on the porphyrin N atoms, which could be explained as a response to the increase in the electronic population on the cobalt, eventually depolarizing the $Co-N_p$ bond. This effect is not observed in the presence of NO, in which case the change in the cobalt atomic charge is not negative but positive, suggesting that charge transfer from the surface is virtually suppressed.

HNO and NO Discrimination with Co(P)-Modified Gold Electrodes. As mentioned in the Introduction, discriminating NO and HNO is a difficult task and it has not been achieved so far in biological samples. Metalloporphyrins are good candidates for the synthesis of gas sensors, and iron porphyrins are known to react with NO. The main difficulty for using iron porphyrins in HNO/NO discrimination is the fact that both the ferric and ferrous states react with both species. Co(P), instead, is selective for either NO or HNO depending on their redox state. We have shown that Co(P)-modified gold electrodes are capable of reacting efficiently with NO only when Co(P) is in the Co^{II} state, while in the Co^{III} state, only reaction with HNO is possible. This behavior possibly relies on the fact that only the $Co^{III}(P)NO^-$ nitroxyl species seem to be stable. In contrast, $Fe^{II}(P)NO$, $Fe^{III}(P)NO$, and also $Fe^{II}(P)HNO$ species have been shown to be stable.[23] Moreover, the discriminative behavior of Co(P) is maintained when the porphyrin is covalently attached to gold electrodes, allowing sensitive electrochemical measurements to be performed. These measurements are aided by a ca. −0.4 V shift of the Co^{III}/Co^{II} redox couple due to interaction with the surface, which allows us to work at a potential in which reaction 7 takes place but reaction 3 does not.

$$(3)\ [Co^{III}(P)]^+ + e^- \longleftrightarrow Co^{II}(P)$$

$$(7)\ [Co^{III}(P)NO]^+ + e^- \longleftrightarrow Co(P)NO$$

Our results show that Co(P)-modified electrodes can react with NO/HNO to yield $Co^{III}(P)NO^-$-modified electrodes and that both $Co^{II}(P)$ and $Co^{III}(P)NO^-$ have at least one electron reduction couple and one electron oxidation couple accessible in aqueous media. Being able to use the modified electrodes in aqueous media is a key issue when developing a selective HNO sensor to be used in biological experiments.

Selective HNO Detection. On the basis of the reactive and electrochemical properties of the Co(P)-modified gold electrodes, we designed a reaction scheme (Scheme 2) for its use in HNO detection. Our results show that the "Co(P) + cystamine"-modified electrode responds to HNO, showing a current intensity after HNO donor addition because of oxidation of $Co^{III}(P)NO^-$. These results make a clear point for the future development of an HNO sensor by using the present strategy for its use in biological media. Once developed, our system could be used directly on the sample in situ without the need for subsequent UV−vis characterization.

Adlayer's robustness of the present device has been verified by exposing the modified surfaces to mild conditions, such as UHV environments, air exposition, and a wide electrochemical potential range. STM surface analysis shows that Co(P) ligands are randomly linked to the Au(111) surface in a lying-down configuration as one- or two-molecule aggregates.

Future work will allow the study of the long-term stability of the electrodes, their quantitative response to HNO, and also their response to other sources of spurious signals such as nitrite and other nitrogen reactive species. Also important is to test the electrode response in aerobic media because, although working under a nitrogen atmosphere in biological in vitro studies is possible, the role of oxygen in HNO chemistry must also be taken into account.

Acknowledgment. This work was financially supported by the University of Buenos Aires, Agencia Nacional de Promoción Científica y Tecnológica (PICT 05-32980 and 06-2396), and CONICET. We also thank Professor F. Battaglini for assistance in the electrochemical measurements.

Supporting Information Available: Synthesis of NO gas (NO) and $Co^{III}(P)NO^-$, supercell of the DFT calculation, measurement of the electrode effective surface area, measurement of the Co(P) gold electrode surface coverage, cyclic voltammograms of $Co^{III}(P)NO^-$ in organic media, height distribution analysis from STM data, effect of cystamine coverage of the Co(P) electrode on the $Co^{III}(P)NO^-$ oxidation signal, estimation of the HNO concentration, selective detection without stirring, and nine supplementary figures. This material is available free of charge via the Internet at http://pubs.acs.org.

(88) Zak, J.; Yuan, H.; Ho, M.; Woo, K. L.; Porter, M. D. *Langmuir* **1993**, *9*, 2772–2774.